Structural and magnetic characterization of multiferroic $(BiFeO_3)_{1-x}(PbTiO_3)_x$ solid solutions

W.-M. Zhu, H.-Y. Guo, and Z.-G. Ye*
Department of Chemistry and 4D LABS, Simon Fraser University, 8888 University Drive, Burnaby, British Columbia, Canada V5A 1S6

(Received 13 December 2007; revised manuscript received 2 April 2008; published 1 July 2008)

A series of multiferroic $(1-x)BiFeO_3-xPbTiO_3$ solid solution ceramics were prepared by solid-state reactions. Structural characterization by x-ray diffraction reveals the existence of a morphotropic phase boundary (MPB) region in this system in which a tetragonal, a rhombohedral, and an orthorhombic phase exist simultaneously with a large tetragonality in the tetragonal phase region. The temperature variation of magnetic moment of the samples with MPB compositions, measured under zero-field cooling (ZFC) mode, shows three anomalies arising from the antiferromagnetic orderings of the rhombohedral, tetragonal, and orthorhombic phases, respectively. The significant difference in antiferromagnetic ordering temperatures of the rhombohedral and tetragonal phases is attributed to the different structural effects on the magnetic interactions between the rhombohedral and the tetragonal phases, and the effect of the magnetic dilution on the magnetic ordering strength. The magnetic phase diagram of the $(1-x)BiFeO_3-xPbTiO_3$ solid solution system was established.

DOI: 10.1103/PhysRevB.78.014401 PACS number(s): 75.30.Kz, 77.84.Dy, 75.50.Ee, 75.30.Cr

I. INTRODUCTION

As a promising candidate for high Curie temperature (T_C=850 °C) high-performance ferroelectric, $BiFeO_3$ was the focus of attention in the 1960s–1970s.[1–11] The structure of its ferroelectric phase[12] shows huge shifts of Bi^{3+} and Fe^{3+} ions, as well as counter rotations of oxygen octahedrons along the ⟨111⟩ direction from the nonferroelectric centrosymmetric cubic structure, giving rise to the R3c space group and a very high spontaneous electric polarization (P_s) calculated from the structural data. $BiFeO_3$ is also a multiferroic material with an antiferromagnetic ordering occurring below the Néel temperature T_N (310–370 °C) (there are discrepancies on T_N, measured by different authors with different methods.[7,8,10,13,14]). Its magnetic structure is of G type[14] with a cycloidal spiral arrangement of the magnetic moments of Fe^{3+} ions,[15] and the canted spins arising from the Dzyaloshinskii-Moriya (D-M) interaction[16,17] give rise to weak ferromagnetism in $BiFeO_3$.[18]

Despite the large ionic displacements in the ferroelectric phase, a P_s value of only 3.5 $\mu C/cm^2$ was measured along the ⟨100⟩ direction (i.e., 6.1 $\mu C/cm^2$ along the ⟨111⟩ polar direction) on the $BiFeO_3$ single crystal at liquid nitrogen temperature,[6] which is much lower than the value expected based on the structural data. Recently, very high values of P_s [55 $\mu C/cm^2$ (Ref. 19) and 150 $\mu C/cm^2$ (Ref. 20)] have been reported on the $BiFeO_3$ thin films. The much higher P_s values measured on thin films over bulk $BiFeO_3$ was initially attributed to the structural factor since the symmetry of the $BiFeO_3$ thin films was found to be tetragonal (P4mm) due to the strain introduced by the $SrRuO_3$ electrode[19] or the substrate,[20] while that of bulk $BiFeO_3$ is rhombohedral (R3c). The Berry phase calculation yielded a P_s of 63.2 $\mu C/cm^2$ along the ⟨100⟩ direction (i.e., 110 $\mu C/cm^2$ along the ⟨111⟩ polar direction) for the tetragonal $BiFeO_3$ (P4mm) while only 6.61 $\mu C/cm^2$ along the ⟨111⟩ direction for the rhombohedral $BiFeO_3$ (R3c).[19] However, in a later improved first-principles calculation, it is shown that the P_s of rhombohedral $BiFeO_3$ can reach 90–100 $\mu C/cm^2$.[21]

In order to obtain large polarization on bulk material, it is necessary to synthesize pure and dense $BiFeO_3$, which can minimize the concentrations of chemical and electronic defects such as oxygen vacancies and Fe^{2+} ions, giving rise to a higher electric resistivity. This turns out to be a difficult task because, first of all, it is very difficult to keep Bi_2O_3 and Fe_2O_3 in stoichiometry during the synthetic process due to the evaporation of Bi_2O_3, which gives rise to the impurity $Bi_2Fe_4O_9$ phase. Although adding excess Bi_2O_3 can avoid the formation of $Bi_2Fe_4O_9$, it could also lead to the formation of the Bi-rich $Bi_{25}FeO_{40}$ impurity phase. Second, $BiFeO_3$ is an incongruent-melting compound; therefore, kinetic cooling process always leads to local deviation from stoichiometry according to the phase diagram of the Bi_2O_3-Fe_2O_3 system.[22] In order to overcome these problems, rapid thermal process (RTP) with a high heating rate (around 100 °C/s) was introduced to reduce the evaporation of the volatile component during the synthesis of the $BiFeO_3$ ceramics,[23] and quenching process following conventional sintering was performed to freeze the metastable $BiFeO_3$ down to room temperature.[24] The polarizations measured on these ceramic samples, although improved, were still significantly lower than that predicted by the first-principles calculations probably because of the incomplete growth of the grains in these processes. Recently, a P_r as high as 60 $\mu C/cm^2$ was measured along the [010] direction (i.e., 100 $\mu C/cm^2$ along the polar ⟨111⟩ direction) of a rhombohedral $BiFeO_3$ single crystal grown from a Bi_2O_3-Fe_2O_3 flux with a low growth temperature of 850 °C,[25,26] indicating that the high polarization is an intrinsic property, rather than a strain-induced effect, of the $BiFeO_3$ phase.

The realization of ultrahigh P_s, the complex mechanisms of the origin of P_s and magnetization, and the fact that $BiFeO_3$ is one of few multiferroic materials[27,28] that could induce magnetoelectric coupling, offering additional degrees of freedom in device design, have given $BiFeO_3$ renewed interests.

Despite its excellent ferroelectric properties and unique multiferroic features, $BiFeO_3$ presents some drawbacks especially in its bulk form. First of all, due to the presence of a

spiral spin arrangement that cancels the macroscopic magnetization arising from the D-M interaction[18] and inhibits the linear magnetoelectric effect,[29] the magnetization and the magnetoelectric effects in $BiFeO_3$ bulk materials are very weak. Second, the extremely high electric coercive field (E_c) of $BiFeO_3$, due to the large energy required for huge ionic shifts during domain switching, limits the ferroelectric applications in bulk forms because a large bipolar voltage is required for full domain switching. In order to improve the multiferroic performance of $BiFeO_3$, different kinds of chemical modifications have been performed. Other materials of perovskite structure were commonly introduced to form solid solutions with $BiFeO_3$. Among them, $PbTiO_3$ appears to be one of the most promising end materials because the introduction of $PbTiO_3$ not only stabilizes the perovskite phase but also forms a morphotropic phase boundary (MPB) with $BiFeO_3$ due to the difference in crystal symmetry between $PbTiO_3$ and $BiFeO_3$. For the compositions around the MPB, E_c is expected to be decreased and piezoelectricity enhanced. The $(1-x)BiFeO_3-xPbTiO_3$ solid solution was first prepared by Venevstev,[30] and later by several other researchers who studied its crystallographic structure and electric properties.[31–40] An MPB was indeed observed in $(1-x)BiFeO_3-xPbTiO_3$ at the composition of $x \approx 0.3$,[31–33,37,38,40] and an unusually large tetragonality (c/a) was found in the tetragonal phase region of this perovskite system.[33,34,38,40] The electric conductivity of the solid solution, although decreased from that of $BiFeO_3$, is still fairly high so that the electric permittivity can only be measured at ultrahigh frequencies.[33] This situation motivated us to study the electric conduction mechanism of the $(1-x)BiFeO_3-xPbTiO_3$ solid solution system by electric impedance spectroscopy, which showed that the electric conduction in $(1-x)BiFeO_3-xPbTiO_3$ arises from the hopping of electrons from Fe^{2+} to Fe^{3+} through oxygen vacancies, which can be effectively decreased by aliovalent ionic substitutions.[38,39] The temperature variations of the dielectric constant were measured up to the ferroelectric Curie point as high as 650 °C in the BF-PT ceramics of MPB composition with aliovalent ionic substitution of Ti^{4+} for Fe^{3+} on the B site[39] and in the BF-PT single crystal of MPB composition grown from Bi_2O_3-PbO flux,[41] because of a decrease in electric conductivity (the low electric conductivity in the BF-PT single crystals is probably due to the suppression of grain boundary and the compensation of oxygen vacancies from the Bi_2O_3-PbO flux). A typical ferroelectric hysteresis loop with P_r of 17 $\mu C/cm^2$ was also displayed in aliovalent ionic substituted ceramics,[39] making BF-PT a high-temperature high-performance ferroelectric material.

It was previously reported that two phases with rhombohedral and tetragonal symmetries coexist in the MPB region of the BF-PT system.[31–33,38,40] However, our recent structural characterization on the BF-PT single crystal with MPB composition revealed extra diffraction peaks in addition to the rhombohedral and tetragonal reflections, which can be indexed by an orthorhombic phase.[41] Since the MPB structure, characterized by a lower symmetry (monoclinic/orthorhombic) phase bridging the rhombohedral and tetragonal phases of the end compounds, is a key feature to the understanding of the enhanced piezoelectric and ferroelectric properties in binary perovskite systems such as PZT,[42] PMN-PT,[43] and PZN-PT,[44] systematic investigation of the MPB phase symmetry and phase components of the BF-PT solid solution system appears to be of relevance to a better understanding of its multiferroic properties.

Adding $PbTiO_3$ to $BiFeO_3$ not only changes the electric properties of $BiFeO_3$ but at the same time also affects the magnetic properties due to the introduction of diamagnetic Ti^{4+} ions onto the B site of the perovskite structure and the consequent change of crystallographic structure. The introduction of Ti^{4+} dilutes the concentration of the paramagnetic Fe^{3+} ions, which is expected to diminish the magnetic ordering strength, leading to a continuous decrease in T_N. The change of crystallographic structure will affect the magnetic interaction by changing the interaction distances and the geometric arrangement of the magnetic ions. With different phases for different compositions as well as an MPB in this system, it is interesting to investigate how the change of structure will affect the magnetic interaction. However, the magnetic properties of this system have not been investigated thoroughly. Fedulov *et al.*[32] reported a preliminary phase diagram of the $(1-x)BiFeO_3-xPbTiO_3$ solid solution in 1964 in which the Néel temperatures were determined by the magnetic measurements using a "homemade" apparatus, which might not be reliable because of the limit of resolution. Moreover, the magnetic measurements were performed only above 0 °C. Recent work by Wang *et al.*[45] on the multiferroic properties of La-modified $Bi(Fe,Ga)FeO_3-xPbTiO_3$ ceramics focused only on samples with compositions x from 0.4 to 0.45 and La concentrations of 10–20 mol %, and only the magnetization as a function of magnetic field of the samples was reported. Our recent work on the single crystal of the $(1-x)BiFeO_3-xPbTiO_3$ solid solution with a composition in the MPB region reveals the coexistence of multiple phases, which seems to affect the magnetic properties.[41] As the multiferroic properties of $BiFeO_3$ experience renewed interests and the $(1-x)BiFeO_3-xPbTiO_3$ solid solution appears to be promising for practical multiferroic applications, we have systematically investigated the structure and magnetic properties, and the structure-property relations of this system in the present work.

II. EXPERIMENT

A. Sample preparation and structural characterization

A series of ceramic samples of the $(1-x)BiFeO_3-xPbTiO_3$ solid solution with composition $x \geq 0.2$ were prepared by solid-state reactions and sintering. The samples are named after their compositions, e.g., 10BF−90PT stands for $0.10BiFeO_3-0.90PbTiO_3$ and so on. The reactants (Bi_2O_3, Fe_2O_3, PbO, and TiO_2) were mixed in stoichiometric amounts in an agate mortar by grinding for 1 h and then pressed into a pellet with a pressure of 1000 kg/cm^2 followed by calcination at 800 °C for 2 h on a platinum plate. After the calcination, the samples were reground and mixed with a few drops of the aqueous polyvinyl alcohol (PVA) binder with a concentration of 6%, and then pressed into pellets with a pressure of 1500 kg/cm^2. The pellets were

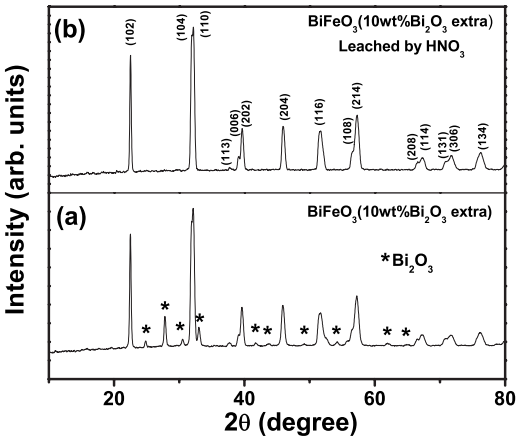

FIG. 1. XRD patterns of $BiFeO_3$ prepared by multistep leach in HNO_3.

subsequently heated at 700 °C for 1 h to eliminate the PVA binder. Afterward, the pellets were sintered in a platinum crucible which was placed in a sealed alumina crucible. The sintering temperature ranges from 1000 °C (for 80BF−20PT) to 1120 °C (for 10BF−90PT), depending on the composition.

Samples with high $BiFeO_3$ amounts, i.e., 90BF−10PT and $BiFeO_3$, showed an impurity phase of $Bi_2Fe_4O_9$, and unreacted Bi_2O_3 after calcination and sintering, if the stoichiometric amounts of reactants were used. In order to avoid the impurity phases, the technique developed by Achenbach *et al.*[46] was used. An excess amount of Bi_2O_3 (10 wt % extra) was added to the starting reactants. The mixture was then calcined at elevated temperatures and/or with extended soaking time, depending on the composition, in order to complete the reactions and to promote the growth of crystal grains. The calcination conditions for $BiFeO_3$ and 90BF−10PT are 800 °C for 48 h, and 950 °C for 2 h, respectively. After the calcination, samples were ground into powder and then followed by multistep leaching in nitric acid with a concentration of 2.5 M. After leaching, the samples were washed thoroughly by distilled water and then heated in furnace at 400 °C for 1 h. Figure 1 shows the x-ray diffraction (XRD) patterns of $BiFeO_3$, prepared by this technique before and after the nitric acid leaching. Pure perovskite phase of $BiFeO_3$ was obtained after leaching by nitric acid.

The XRD was carried out by a Philips PW-1730 diffractometer on sintered ($x \geq 0.2$) and calcined ($BiFeO_3$ and 90BF−10PT) ceramic samples with a step size of 0.02°. The XRD data were then used to calculate the lattice parameters of these samples by using XLAT software. The XRD profiles of samples with MPB compositions were deconvoluted by a combination of Lorentzian and Gaussian functions using the PEAKFIT v4.00 software (Jandel Scientific Corp.).

B. Characterization of magnetic properties

Magnetic moments of the $(1-x)BiFeO_3-xPbTiO_3$ ceramics were measured by a superconducting quantum interference device (SQUID) (Quantum Design MPMS XL) magnetometer. Temperature variation of the magnetic moment was measured under zero-field cooling (ZFC) mode. The samples were preheated at 500 °C in a furnace before the ZFC measurements. "Low-temperature" measurements (2–400 K) were carried out on all samples in the following way: the samples were heated up to 400 K and then cooled down to 2 K without magnetic field, and afterward, the magnetic moment was measured upon heating with a magnetic field of 100 Oe. "High-temperature" measurements (400–690 K with an attached oven) were carried out on samples with composition $x \leq 0.31$ only, which were heated up to 690 K and then cooled down to 400 K without magnetic field. Afterward, the magnetic moment was measured upon heating at a magnetic field of 1 T (a higher magnetic field is applied because of the decreased resolution in the SQUID when using an oven). The magnetic moments obtained by both the high-temperature and the low-temperature measurements were normalized by the mole number of the sample and the magnetic field applied. The dependences of magnetization on magnetic field (magnetic hysteresis loops) of 45BF−55PT and $BiFeO_3$ were measured upon cooling at different temperatures after the sample was preheated up to 500 °C in a furnace without magnetic field.

III. STRUCTURAL CHARACTERIZATION

Figure 2 shows the XRD patterns of the $(1-x)BiFeO_3-xPbTiO_3$ ceramics. Starting from $BiFeO_3$ ($x=0$) with the increase in x, a change from the rhombohedral phase to a mixture of morphotropic phases and then to the tetragonal phase is evidenced, indicating a morphotropic phase boundary (MPB) region in this system, which covers the compositions from $x=0.20$ to $x=0.28$. The calculated room-temperature lattice parameters, as a function of composition in the single phase regions, are shown in Fig. 3. The lattice parameters of the tetragonal phase were calculated based on the P4mm symmetry. An unusually large tetragonality (c/a) is found for $x=0.31-1$, which decreases with the increase in x from 1.187 for $x=0.31$ to 1.06 for $x=1$ [Fig. 3(b)]. The lattice parameters of the rhombohedral phase were calculated based on the R3c symmetry because, according to the electron-diffraction patterns, the rhombohedral $(1-x)BiFeO_3-xPbTiO_3$ still adopts the same counter rotation of oxygen octahedrons (along the ⟨111⟩ direction) as in $BiFeO_3$ although the rotation angle decreases with the increase in x.[37] This result is different from the one reported in Refs. 32 and 33, where the lattice parameters of the rhombohedral phase were calculated based on the R3m symmetry that arises from the displacement of A and B site cations along the ⟨111⟩ direction only. The samples with MPB compositions show strong overlaps of the diffraction peaks of the morphotropic phases. Therefore, their XRD profiles were deconvoluted to analyze the MPB phase components.

Figure 4 gives the deconvolution results of the XRD profiles for the MPB compositions at the $(110)_{cub}$ peak position, which show the highest intensity. 83BF–17PT is of pure rhombohedral phase and 69BF–31PT is of pure tetragonal phase. The XRD profiles of 80BF–20PT, 75BF–25PT, and 72BF–28PT can be deconvoluted into seven peaks, as shown in Figs. 4(b)–4(d), and the insets therein. Based on the evo-

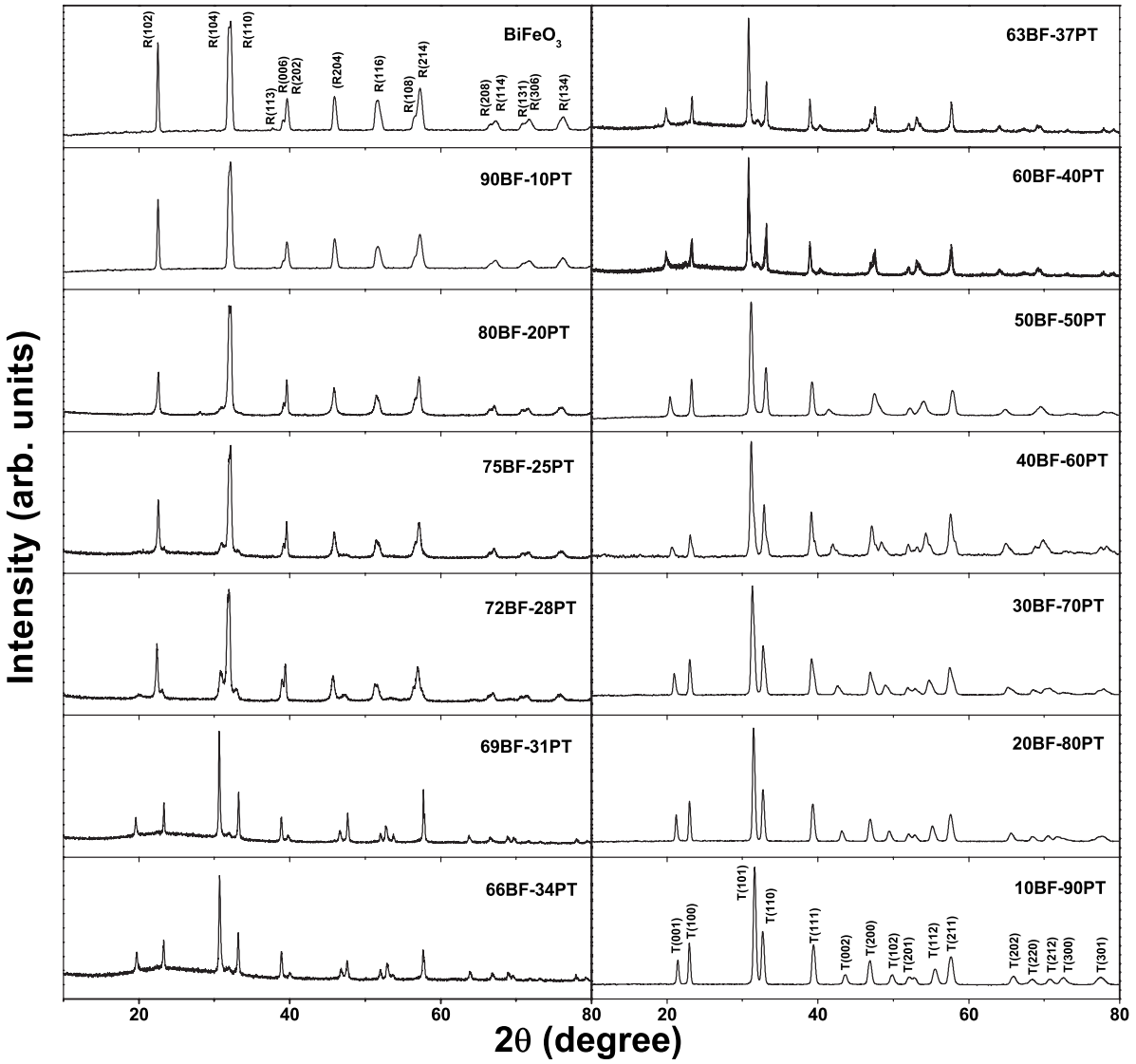

FIG. 2. XRD patterns of the $(1-x)BiFeO_3-xPbTiO_3$ solid solution ceramics.

lution of the XRD profiles with respect to composition, peaks 1 and 7 result from the tetragonal (101) and (110) splittings, and peaks 3 and 5 from the rhombohedral (104) and (110) splittings. The deconvolutions of the rest of the peaks, i.e., peaks 2, 4, and 6, suggest the presence of an orthorhombic phase, which has a triplet splitting from the $(110)_{cub}$ peak. In order to confirm this, the full XRD profile of 72BF−28PT was deconvoluted, as shown in Fig. 5. Each of the deconvoluted peaks was indexed, and the lattice parameters of the tetragonal, orthorhombic, and rhombohedral phases were calculated based on the indexed peaks (Table I), which give rise to converged results. It confirms the existence of an orthorhombic phase together with the tetragonal and rhombohedral phases in the samples with MPB compositions.

Our result is different from that of a recent structural study on the BF-PT system in which the coexistence of rhombohedral and tetragonal phases was reported in the MPB region.[40] However, it is consistent with the electron-diffraction study of the BF-PT ceramics with MPB composition,[37] in which, in addition to the rhombohedral and tetragonal reflections, incommensurate reflections were observed. It implies the presence of a new phase with a lower symmetry. It should be pointed out that, in Ref. 40, only the structural refinement result of the pure tetragonal phase sample (i.e., $0.69BiFeO_3-0.31PbTiO_3$) was reported and the T001 peak of the MPB composition sample [Fig. 2(b) of Ref. 40] exhibits a shoulder on the left side, which clearly indicates the presence of an additional diffraction peak. Therefore, more careful analysis of the diffraction patterns in Ref. 40 would have revealed the presence of a new phase of lower symmetry in the MPB region.

The monoclinic phase, as an intermediate state between the rhombohedral and tetragonal phases, was found in the MPB region of some relevant perovskite solid solutions such as PZT (Ref. 42) and PMN-PT (Ref. 43). However, our structural analysis showed that the $(110)_{cub}$ peak set of the MPB compositions (Fig. 4) can be well fitted by an orthorhombic phase with a triplet splitting, together with a tetragonal phase with a doublet splitting and a rhombohedral phase

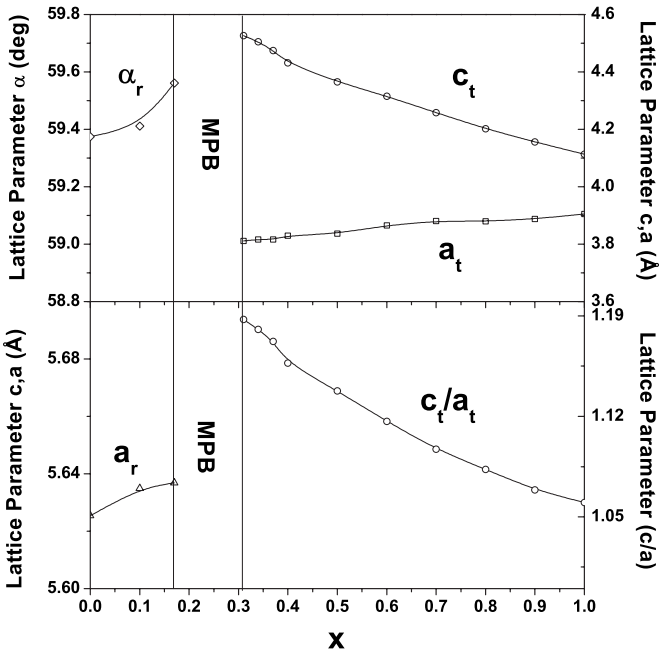

FIG. 3. Variation of the lattice parameters as a function of composition in the $(1-x)BiFeO_3-xPbTiO_3$ solid solution system.

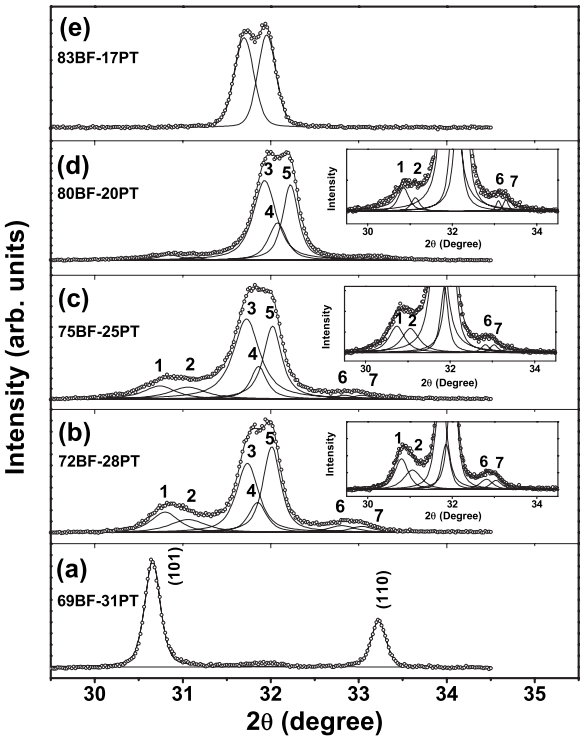

FIG. 4. Deconvolution results of the XRD profiles [split from the cubic (110) peak] of ceramic samples with the MPB compositions for the $(1-x)BiFeO_3-xPbTiO_3$ solid solution. Dots indicate the experimental XRD data and solid lines the fitting results.

with a doublet splitting. A monoclinic phase would result in five peaks for $(110)_{cub}$, which could not fit our XRD patterns.

Theoretical calculation showed that the presence of a monoclinic phase in the MPB region and the associated polarization rotation are favored by a lower free energy of the system when going through a tetragonal-monoclinic-rhombohedral pathway than, otherwise, through a tetragonal-orthorhombic-rhombohedral pathway. Hence, the tetragonal-monoclinic-rhombohedral phase sequence is preferred with the change of composition across the MPB.[47] However, this calculation was based on $BaTiO_3$, which has a very small lattice distortion in its ferroelectric tetragonal phase ($c/a=1.01$). In the present case of BF-PT, the lattice distortion in the ferroelectric phase is much greater (e.g., $c/a=1.187$ for $0.69BiFeO_3-0.31PbTiO_3$), the symmetry of the rhombohedral phase (R3c, due to the counter rotation of the oxygen octahedra) is different from that of $BaTiO_3$ (R3m), and moreover, there exist spin interactions. These peculiar features could explain the different phase sequence through the pathway of tetragonal-orthorhombic-rhombohedral across the MPB for the BF-PT system, as revealed by our structural analysis. This result suggests that further first-principles study on the BF-PT system is needed to confirm the MPB phase sequence.

IV. MAGNETIC CHARACTERIZATION

Figure 6 shows the temperature variation of magnetic moment for both high-temperature (400–690 K) and low-temperature measurements (2–400 K) of the $(1-x)BiFeO_3-xPbTiO_3$ ceramics with composition x from 0 to 0.31. For the high-temperature measurements [Fig. 6(a)], the temperature dependence of the magnetic moment of $BiFeO_3$ shows a peak at $T_{N-r}=630$ K, which is in agreement with the T_N of $BiFeO_3$ previously reported,[7,13,14] indicating the paramagnetic-antiferromagnetic phase transition. With the increase in x, this peak diminishes into a bump and finally disappears in 69BF−31PT and the corresponding antiferromagnetic ordering temperature (T_{N-r}) decreases. T_{N-r} covers the composition range from $x=0$ to $x=0.28$ [Fig. 6(a)], which is identical to that for the rhombohedral phase (Figs. 3 and 4). Therefore, T_{N-r} indicates the antiferromagnetic ordering temperature of the rhombohedral phase of the $(1-x)BiFeO_3-xPbTiO_3$ solid solution.

In addition to the anomaly at T_{N-r}, two more anomalies, at T_{N-t1} and T_{N-o}, are observed on the low-temperature magnetic moment [Fig. 6(b)] for the samples with MPB compositions, i.e., 80BF−20PT, 75BF−25PT, and 72BF−28PT. This reveals that, in the whole temperature range of measurement, the samples with MPB compositions exhibit three magnetic transitions. According to the structural analysis results in Sec. III, three phases: rhombohedral, orthorhombic, and tetragonal, exist simultaneously in the MPB region. Therefore, it is reasonable to suggest that each of these phases undergoes an antiferromagnetic ordering at a distinct temperature, leading to an anomaly on the temperature dependence of magnetic moment. Both T_{N-t1} and T_{N-o} decrease with the increase in x across the MPB region.

With the further increase in composition parameter x into the tetragonal phase region, i.e., for samples with x from 0.31 to 0.37, only one anomaly can be observed on the temperature variation of the magnetic moment whose corresponding temperature (T_{N-t2}) decreases with the increase in x (Fig. 7). However, for the samples with x from 0.40 to 0.70 in addi-

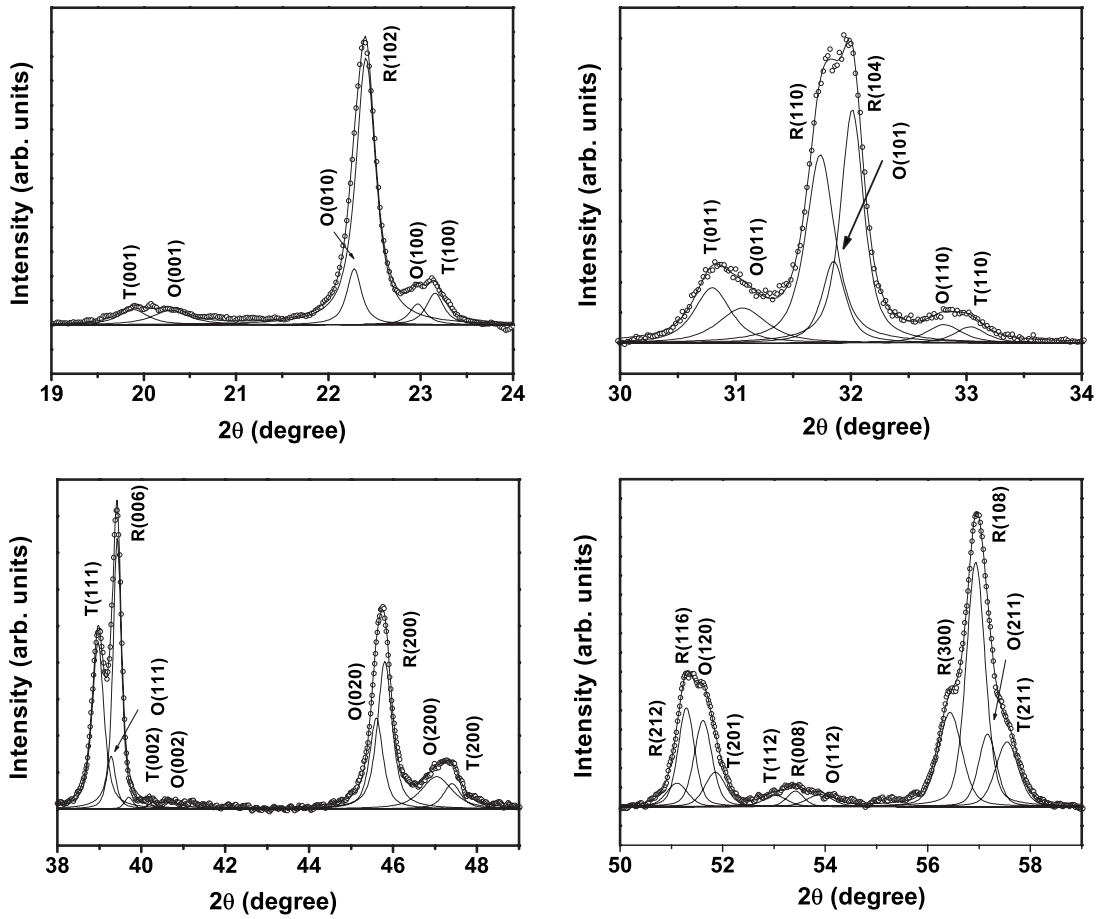

FIG. 5. Deconvolution of the pseudocubic (a) (100) peak, (b) (110) peak, (c) (111) and (200) peaks, and (d) (201) and (211) peaks from the XRD of the 72BF−28PT. Dots are experimental data and solid lines are the fitting results.

tion to the anomaly $T_{N\text{-}t2}$ (inset of Fig. 8), one more anomaly appears at a lower temperature T_C (Fig. 8). T_C increases first with the increase in x, reaches the maximum value of 23 K in 45BF−55PT, and then decreases with further increase in x.

The magnetization (M) of the tetragonal 45BF−55PT as a function of magnetic field (H) measured at different temperatures is shown in Fig. 9. With the decrease in temperature, the M vs H relation becomes nonlinear with a remnant magnetization close to zero below $T_{N\text{-}t2}$ of 70 K [Fig. 9(a)]. This means that $T_{N\text{-}t2}$ is the antiferromagnetic ordering temperature of the tetragonal phase in this solid solution. At 10 K, a hysteresis loop with remnant magnetization appears clearly [Fig. 9(b)], which becomes more enhanced at 2 K [Fig. 9(c)], indicating a ferromagnetic state in 45BF−55PT below T_C. In contrast to this, the M vs H relation of pure $BiFeO_3$ ceramic remains linear with almost no remnant magnetization down to 2 K [Fig. 9(d)].

TABLE I. Lattice parameters of the tetragonal, orthorhombic, and rhombohedral phases in 72BF−28PT.

	Tetragonal	Orthorhombic	Hexagonal (Rhombohedral)[a]	
			Hexagonal	Rhombohedral
a(Å)	3.8315(32)	3.8606(26)	5.6300(83)	5.6074
b(Å)		3.9784(20)		
c(Å)	4.4732(73)	4.3039(12)	13.0764(80)	
c/a	1.1675			
α(°)				60.2704

[a]The rhombohedral lattice parameters are converted from the hexagonal lattice parameters based on the R3c space group.

It should be noted that the magnetic anomaly at T_C appears only in the samples of compositions with BF:PT ratio around 50:50, which favors the formation of chemically ordered microregions (with e.g., superlattices of the ordered Fe^{3+} and Ti^{4+} ions on the B site). In the chemically ordered microregions, the spiral spin modulation initially existing in $BiFeO_3$ is expected to be disturbed and completely disappear. The D-M type interaction is enhanced due to the long coupling distance between the neighboring Fe^{3+} ions, which interact with each other via long-range superexchange of the Fe^{3+}-O-Ti-O-Fe^{3+} pathway, giving rise to a low magnetic onset temperature. This results in uncompensated magnetization in those chemically ordered microregions, which we call magnetic nanoclusters (MNCs). The freezing of theses MNCs gives rise to the residual magnetization, hence, a weak ferromagnetic state.[48] The freezing out of the MNCs is confirmed by the Vogel-Fulcher fitting of the ac magnetic susceptibility of 45BF-55PT (not shown here), which gives rise to a freezing temperature of 21 K, close to the T_C. It is also confirmed by the splitting between the field-cooled and

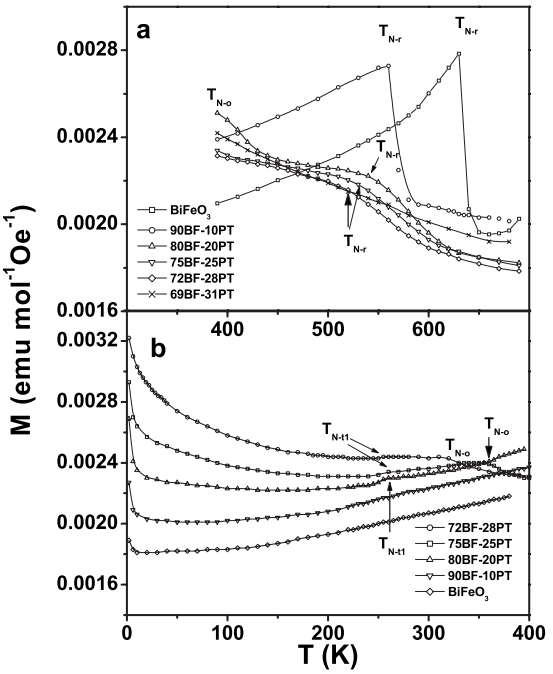

FIG. 6. Temperature dependences of magnetic moment of the $(1-x)BiFeO_3-xPbTiO_3$ system (for composition $x=0-0.31$): (a) high-temperature (using oven) and (b) low-temperature measurements.

zero-field cooled M vs T curves of 45BF-55PT below T_C, which indicates an ergodicity breaking due to the freezing of the MNCs.[48] Thus, the freezing of the MNCs indeed leads to the weak ferromagnetic state below T_C.

With further increase in $PbTiO_3$ content (i.e., >70 mol%), this weak ferromagnetic state disappears because of the significant dilution of the Fe^{3+} concentration, which reduces the size and number of chemically ordered microregion, and weakens the magnetic interactions.

For 10BF−90PT and 20BF−80PT, no magnetic anomaly is observed on their temperature variations of magnetic susceptibility (Fig. 10). However, extrapolation of the linear portion (Curie-Weiss law) of the reciprocal magnetic susceptibility to the temperature axis gives rise to a negative Curie-

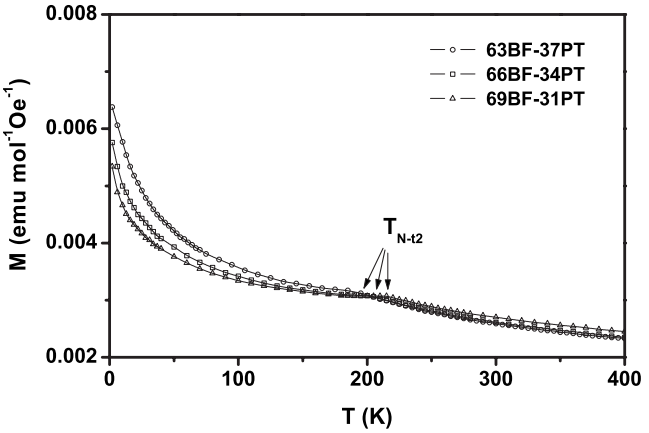

FIG. 7. Temperature dependence of the magnetic moment of the $(1-x)BiFeO_3-xPbTiO_3$ system (for composition $x=0.31-0.37$).

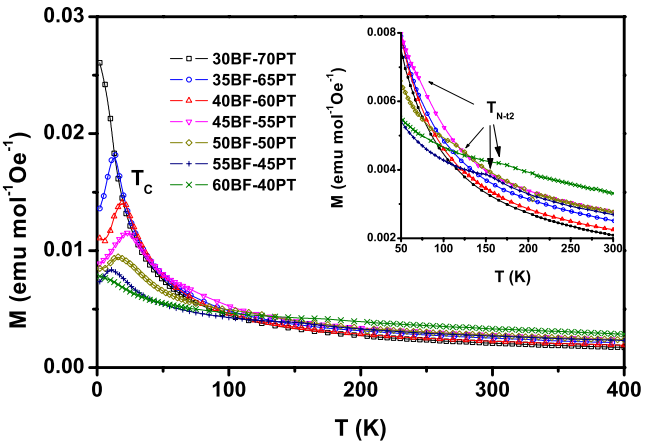

FIG. 8. (Color online) Temperature dependence of the magnetic moment of the $(1-x)BiFeO_3-xPbTiO_3$ system (for composition $x=0.40-0.70$).

Weiss temperature (T_{CW}) (Fig. 10), indicating that the magnetic coupling in these two samples is still mainly of antiferromagnetic nature at low temperatures but the concentration of the magnetic Fe^{3+} ions has become too low for a long-range magnetic ordering to occur.

Based on the above results, the magnetic phase diagram of the $(1-x)BiFeO_3-xPbTiO_3$ system has been established in terms of temperature and composition, as shown in Fig. 11. It defines the various magnetic phases and the corresponding magnetic transition temperatures. T_{N-r}, T_{N-o}, and T_{N-t} (T_{N-t1} and T_{N-t2}) are the antiferromagnetic ordering temperatures of the rhombohedral, orthorhombic, and tetragonal phases (the orthorhombic phase only appears in the MPB region), respectively. In addition to the antiferromagnetic ordering temperatures for different phases, the magnetic phase diagram also shows the low-temperature ferromagnetic transition at T_C in the tetragonal phase region, arising from the long-range superexchange of Fe^{3+}-O-Ti-O-Fe^{3+} in the chemically ordered microregions.

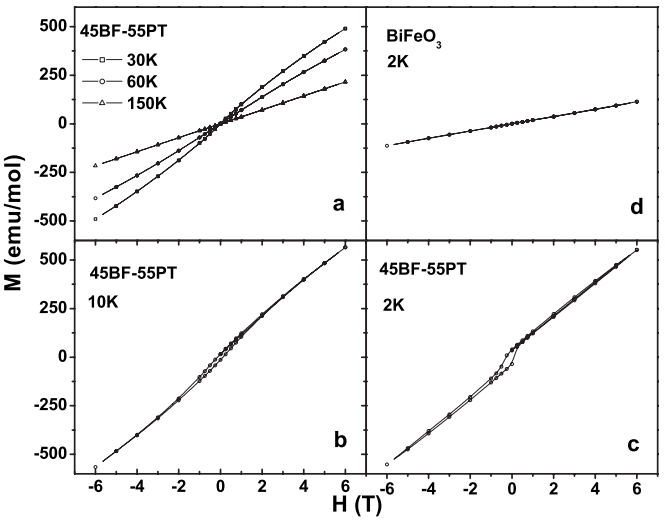

FIG. 9. Magnetization (M)as a function of bipolar field (H) for 45BF−55PT measured at difference temperatures (a-c), and for BF measured at 2 K.

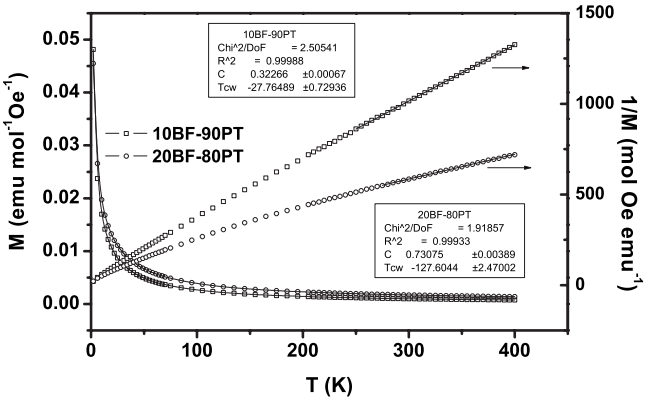

FIG. 10. Temperature dependences of the magnetic susceptibility (χ) and their Curie-Weiss fitting results of 10BF−90PT and 20BF−80PT.

V. DISCUSSION

Compared with the phase diagram of the $(1-x)BiFeO_3-xPbTiO_3$ solid solution reported in Ref. 32, the current magnetic phase diagram (Fig. 11) shows a comparable antiferromagnetic ordering temperature in the rhombohedral phase region but a much lower antiferromagnetic ordering temperature in the tetragonal phase region. In order to understand the reasons for such a discrepancy, and the remarkable difference in antiferromagnetic ordering temperatures between the tetragonal and the rhombohedral phases observed in the present phase diagram, we need to examine the factors that affect the antiferromagnetic ordering temperatures in this system.

The $(1-x)BiFeO_3-xPbTiO_3$ solid solution is a magnetically diluted system from $BiFeO_3$. Although the dilution makes some of the magnetic ions to have less than six magnetic neighbors, it does not change the nature of the magnetic interaction of $BiFeO_3$, i.e., in $(1-x)BiFeO_3-xPbTiO_3$, each Fe^{3+} ion couples primarily antiferromagnetically with all its neighboring Fe^{3+} ions. Therefore, the magnetic ordering in this system arises from the cooperative magnetic interaction of Fe^{3+}-O-Fe^{3+}, which "connects" those effective magnetic ions through superexchange by the "bonds" of Fe^{3+}-O-Fe^{3+}, forming a network, or at least a backbone, percolating a grain. The magnetic ordering temperature is the temperature at which the cooperative magnetic interaction sets up. The cooperative magnetic interaction correlates each of the spins in the network or backbone. Such an onset of magnetic ordering gives rise to a stronger magnetic response, which is seen as an anomaly on the temperature variation of magnetic moment. Above the magnetic ordering temperature, the network or backbone collapses because of the breakdown of some critical bonds, which leads to the formation of magnetic clusters. Consequently, the cooperative magnetic interaction disappears. Nevertheless, magnetic interaction still subsists locally in the magnetic clusters until the temperature increases to a critical point at which no magnetic interaction can take place between any of the two magnetic neighboring ions because of thermal agitation, and thereby the material becomes paramagnetic.

Based on the above arguments, the magnetic ordering temperature is obviously related to the concentration of the magnetic ions in the material: the higher the concentration of the magnetic ion, the higher the probability to form a network or backbone percolating a grain, and the stronger the strength of the network or backbone with respect to thermal agitation, which gives rise to a higher magnetic ordering temperature. Since whether or not the magnetic interaction between two neighboring magnetic ions can setup at a certain temperature depends on the distance between them, the magnetic ordering temperature should also be related to the "bond" length in the network or backbone: the longer the bond length, the lower the ordering temperature.

In the present case, the lattice parameter c of the tetragonal phase is larger than a (Fig. 3), which means that, in the tetragonal phase, the average atomic distance of Fe^{3+}-O-Fe^{3+} along the c direction is larger than that along a and b directions. This gives rise to a weaker magnetic interaction along the c direction than along the a and b directions, and therefore, the bonds along the c direction are the critical bonds, which break first with the increase in temperature, making the network or backbone collapse. Therefore, in the tetragonal phase, the lattice parameter c determines the "critical coupling distance" of the cooperative magnetic interaction for the magnetic ordering. In the rhombohedral phase, the average atomic distance of Fe^{3+}-O-Fe^{3+} is equal to $(\sqrt{2}/2)a$ along the three directions, where a is the lattice parameter of the rhombohedral R3c unit cell, which determines the critical coupling distance [the hexagonal unit cell size of the R3c rhombohedral phase doubles that of R3m along the hexagonal [0001] direction (i.e., the [111] direction of the rhombohedral phase), as illustrated in Fig. 12]. The orthorhombic phase appears only in the MPB region. The lattice parameter c of the orthorhombic phase is larger than a and b. Therefore, c determines the critical coupling distance of the orthorhombic phase.

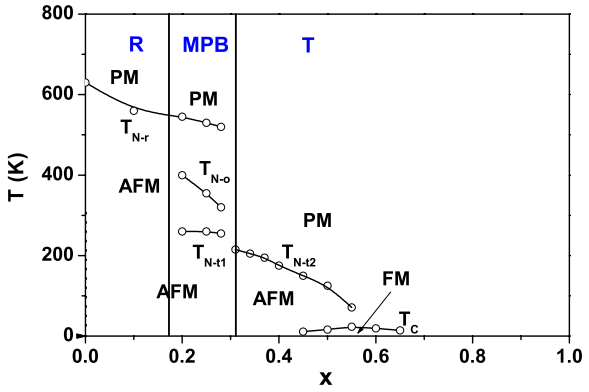

FIG. 11. (Color online) Magnetic phase diagram of the $(1-x)BiFeO_3-xPbTiO_3$ system, which delimits the following phase regions and transition temperatures: R—rhombohedral phase, T—tetragonal phase, PM—paramagnetic phase, FM—ferromagnetic phase, AFM—antiferromagnetic phase, T_{N-r}—antiferromagnetic ordering temperature of the rhombohedral phase, T_{N-t1}—antiferromagnetic ordering temperature of the tetragonal phase (MPB region), T_{N-t2}—antiferromagnetic ordering temperature of the tetragonal phase (tetragonal phase region), T_{N-o}—antiferromagnetic ordering temperature of orthorhombic phase (MPB region), and T_C—ferromagnetic state transition temperature.

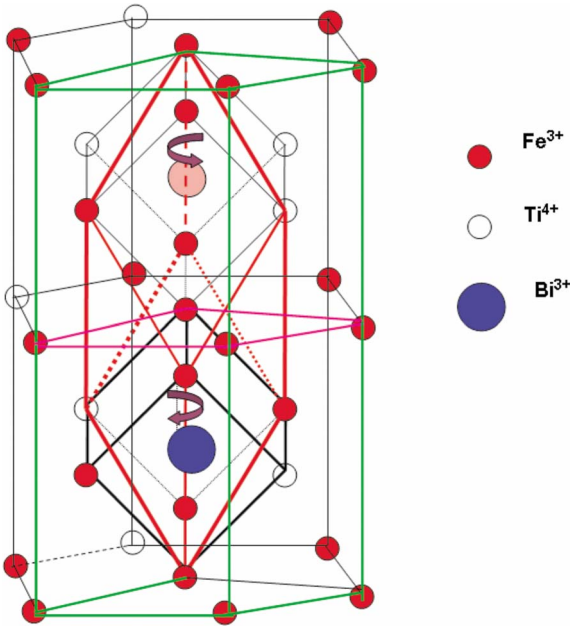

FIG. 12. (Color online) Illustration of the rhombohedral unit cell with R3c symmetry (red lines) of the $(1-x)BiFeO_3-xPbTiO_3$ solid solution. In comparison, the R3m rhombohedral unit cell is shown in solid black lines. The corresponding hexagonal unit cell of R3c (green lines) and R3m (purple and green lines) are also presented.

In the MPB region, three phases exist simultaneously. Taking 72BF−28PT as an example, the lattice parameter c of the tetragonal phase is 4.4732 Å, that of the orthorhombic phase is 4.3039 Å, and $(\sqrt{2}/2)a$ of the rhombohedral phase is 3.9656 Å. This indicates that the critical coupling distance of the tetragonal phase is the largest and the critical coupling distance of the orthorhombic phase is larger than that of the rhombohedral phase. Therefore, the antiferromagnetic ordering temperature of the tetragonal phase is much lower than that of the rhombohedral phase and the antiferromagnetic ordering temperature of the orthorhombic phase is in between them.

In the tetragonal phase region with the increase in x, although the lattice parameter c, i.e., the critical coupling distance, decreases (Fig. 3), the magnetic ordering temperature still decreases because the decrease in the concentration of magnetic ions prevails.

In the present magnetic phase diagram, the antiferromagnetic ordering temperature T_N of the rhombohedral phase is close to, although that of the tetragonal phase is much lower than, the Néel temperatures reported in Ref. 32, where T_N was determined by the temperature dependence of the specific spontaneous magnetization (σ_s) and assigned to the temperature at which σ_s became zero. The Néel temperature determined in this way does not reflect the long-range antiferromagnetic ordering because the σ_s does not disappear with the breakdown of the long-range antiferromagnetic ordering and it persists as long as the local magnetic interaction of Fe^{3+}-O-Fe^{3+} exists. Therefore, the Néel temperature determined in this way is usually higher than the actual antiferromagnetic ordering temperature. Nevertheless, in the rhombohedral phase region, the Néel temperature reported in Ref. 32 is close to the antiferromagnetic ordering temperature observed in the present work. This can be explained based on the different effects of magnetic dilution on the magnetic ordering temperatures for the compositions of low and high concentrations of magnetic ions, respectively. When the dilution is low, the long-range antiferromagnetic ordering can be setup in the form of network, which is relatively strong because the breakdown of some connections will not significantly affect the long-range ordering. Therefore, the magnetic ordering temperature and the temperature at which σ_s disappears are quite close. When the dilution is high, the long-range antiferromagnetic ordering might be set up in the form of a chain instead of a network, which is more vulnerable to thermal agitation, giving rise to a lower long-range magnetic ordering temperature than the temperature at which σ_s disappears. Based on this reasoning, both the structural effect discussed above and the different effects of magnetic dilution on magnetic ordering strength in different compositions are responsible for the much lower antiferromagnetic ordering temperature in the tetragonal phase than in the rhombohedral phase.

VI. CONCLUSIONS

The structural characterization by means of x-ray diffraction and phase analysis has revealed the existence of a morphotropic phase boundary region in the multiferroic $(1-x)BiFeO_3-xPbTiO_3$ solid solution system. In the MPB region, three phases: tetragonal, rhombohedral, and orthorhombic, exist simultaneously.

The magnetic characterization by means of SQUID has allowed us to establish the magnetic phase diagram of the multiferroic $(1-x)BiFeO_3-xPbTiO_3$ solid solution system. In accordance with the structural analysis, the temperature variations of the magnetic moment of the system in the MPB region show three anomalies corresponding to the antiferromagnetic ordering temperatures of the tetragonal, rhombohedral, and orthorhombic phases, respectively. The remarkable difference in the antiferromagnetic ordering temperatures between the tetragonal and the rhombohedral phases was explained based on the structural effect on the magnetic interactions, and the effect of magnetic dilution on magnetic ordering strength.

ACKNOWLEDGMENTS

This work was supported by the U.S. Office of Naval Research (Grant No. N00014-06-1-0166) and by the National Science and Engineering Research Council of Canada (NSERC). The authors thank A. A. Bokov for helpful discussion.

*Corresponding author. Fax: 1-778-782-3765. zye@sfu.ca

[1] N. N. Krainik, N. P. Khuchua, V. V. Zhdanova, and V. A. Evseev, Sov. Phys. Solid State **8**, 654 (1966).
[2] Y. Y. Tomashpolskii and Y. N. Venevtsev, Sov. Phys. Crystallogr. **12**, 18 (1967).
[3] Y. Y. Tomashpolskii, Y. N. Venevtsev, and G. S. Zhdanov, Sov. Phys. Crystallogr. **12**, 209 (1967).
[4] I. G. Ismailzade, Sov. Phys. Dokl. **11**, 747 (1967).
[5] C. Michel, J. M. Moreau, G. D. Achenbach, R. Gerson, and W. J. James, Solid State Commun. **7**, 701 (1969).
[6] J. R. Teague, R. Gerson, and W. J. James, Solid State Commun. **8**, 1073 (1970).
[7] J. M. Moreau, C. Michel, R. Gerson, and W. J. James, J. Phys. Chem. Solids **32**, 1315 (1971).
[8] C. Blaauw and F. van der Woude, J. Phys. C **6**, 1422 (1973).
[9] A. J. Jacobson and B. E. F. Fender, J. Phys. C **8**, 844 (1975).
[10] P. Fischer, M. Połomska, I. Sosnowska, and M. Szymański, J. Phys. C **13**, 1931 (1980).
[11] S. A. Fedulov, Sov. Phys. Dokl. **6**, 726 (1962).
[12] F. Kubel and H. Schmid, Acta Crystallogr., Sect. B: Struct. Sci. **46**, 698 (1990).
[13] G. Smolenskii, Sov. Phys. Solid State **2**, 2651 (1961).
[14] S. V. Kiselev, R. P. Ozerov, and G. S. Zhdanov, Sov. Phys. Dokl. **7**, 742 (1963).
[15] I. Sosnowska, T. Peterlin-Neumaier, and E. Steichele, J. Phys. C **15**, 4835 (1982).
[16] I. E. Dzialoshinskii, Sov. Phys. JETP **5**, 1259 (1957).
[17] T. Moriya, Phys. Rev. **120**, 91 (1960).
[18] C. Ederer, and N. A. Spaldin, Phys. Rev. B **71**, 060401(R) (2005).
[19] J. Wang, J. B. Neaton, H. Zheng, V. Nagarajan, S. B. Ogale, B. Liu, D. Viehland, V. Vaithyanathan, D. G. Schlom, U. V. Waghmare, N. A. Spaldin, K. M. Rabe, M. Wuttig, and R. Ramesh, Science **299**, 1719 (2003).
[20] K. Y. Yun, D. Ricinschi, T. Kanashima, M. Noda, and M. Okuyama, Jpn. J. Appl. Phys., Part 2 **43**, L647 (2004).
[21] J. B. Neaton, C. Ederer, U. V. Waghmare, N. A. Spaldin, and K. M. Rabe, Phys. Rev. B **71**, 014113 (2005).
[22] A. Maitre, M. Francois, and J. C. Gachon, J. Phase Equilibria and Diffusion **25**, 59 (2004).
[23] Y. P. Wang, L. Zhou, M. F. Zhang, X. Y. Chen, J.-M. Liu, and Z. G. Liu, Appl. Phys. Lett. **84**, 1731 (2004).
[24] S. T. Zhang, M. H. Lu, D. Wu, Y. F. Chen, and N. B. Ming, Appl. Phys. Lett. **87**, 262907 (2005).
[25] D. Lebeugle, D. Colson, A. Forget, and M. Viret, Appl. Phys. Lett. **91**, 022907 (2007).
[26] D. Lebeugle, D. Colson, A. Forget, M. Viret, P. Bonville, J. F. Marucco, and S. Fusil, Phys. Rev. B **76**, 024116 (2007).
[27] N. A. Hill, J. Phys. Chem. B **104**, 6694 (2000).
[28] N. A. Hill and A. Filippetti, J. Magn. Magn. Mater. **242-245**, 976 (2002).
[29] Y. F. Popov, A. K. Zvezdin, G. P. Vorob'ev, A. M. Kadomtseva, V. A. Murashev, and D. N. Rakov, JETP Lett. **57**, 69 (1993).
[30] Y. N. Venevtsev, Sov. Phys. Crystallogr. **5**, 594 (1960).
[31] S. A. Fedulov, Y. N. Venevtsev, G. S. Zhdanov, G. E. Smazhevskaya, and I. S. Rez, Sov. Phys. Crystallogr. **7**, 62 (1962).
[32] S. A. Fedulov, P. B. Ladyzhinskii, I. L. Pyatigorskaya, and Y. N. Venevtsev, Sov. Phys. Solid State. **6**, 375 (1964).
[33] R. T. Smith, G. D. Achenbach, R. Gerson, and W. J. James, J. Appl. Phys. **39**, 70 (1968).
[34] V. V. S. S. Sai Sunder, A. Halliyal, and A. M. Umarji, J. Mater. Res. **10**, 1301 (1995).
[35] J.-R. Cheng, N. Li, and L. E. Cross, J. Appl. Phys. **94**, 5153 (2003).
[36] J.-R. Cheng and L. E. Cross, J. Appl. Phys. **94**, 5188 (2003).
[37] D. I. Woodward, I. M. Reaney, R. E. Eitel, and C. A. Randall, J. Appl. Phys. **94**, 3313 (2003).
[38] W. M. Zhu and Z.-G. Ye, Ceram. Int. **30**, 1435 (2004).
[39] W.-M. Zhu and Z.-G. Ye, Appl. Phys. Lett. **89**, 232904 (2006).
[40] S. Bhattacharjee, S. Tripathi, and D. Pandey, Appl. Phys. Lett. **91**, 042903 (2007).
[41] W.-M. Zhu and Z.-G. Ye, J. Mater. Res. **22**, 2136 (2007).
[42] B. Noheda, D. E. Cox, G. Shirane, R. Guo, B. Jones, and L. E. Cross, Phys. Rev. B **63**, 014103 (2000).
[43] Z.-G. Ye, B. Noheda, M. Dong, D. E. Cox, and G. Shirane, Phys. Rev. B **64**, 184114 (2001).
[44] D. La-Orauttapong, B. Noheda, Z. G. Ye, P. M. Gehring, J. Toulouse, D. E. Cox, and G. Shirane, Phys. Rev. B **65**, 144101 (2002).
[45] N. Wang, J. Cheng, A. Pyatakov, A. K. Zvezdin, J. F. Li, L. E. Cross, and D. Viehland, Phys. Rev. B **72**, 104434 (2005).
[46] G. D. Achenbach, W. J. James, and R. Gerson, J. Am. Ceram. Soc. **50**, 437 (1967).
[47] H. Fu and R. Cohen, Nature (London) **403**, 281 (2000).
[48] W.-M. Zhu, H.-Y. Guo, and Z.-G. Ye (unpublished).